# Design, construction, quality control and performance study with cosmic rays of modules for the LHCb electromagnetic calorimeter

A. Aref'ev[a], S. Barsuk[b], I. Belyaev[a], B. Bobchenko[a], L. Camilleri[c], V. Egorychev[a], Yu. Gilitsky[d], A. Golutvin[a], O. Gouchtchine[a], I. Korolko[a], T. Kvaratskheliya[a], I. Machikhilian[c], M. Martemiyanov[a], E. Melnikov[a], A. Morozov[a], M. Prokudin[a], D. Roussinov[a], V. Rusinov[a], A. Schopper[c], S. Shuvalov[e], A. Soldatov[d], E. Tarkovsky[a], K. Voronchev[a]

[a] Institute for Theoretical and Experimental Physics
B. Cheremushkinskaya, 25, Moscow 117259, Russia

[b] Laboratoire de l'Accélérateur Linéaire, Université Paris-Sud 11
Bâtiment 200, 91898 Orsay, France

[c] European Organization for Nuclear Research
CERN, CH-1211, Geneve 23, Switzerland

[d] Institute for High Energy Physics
Protvino, Moscow region, 142281, Russia

[e] German Electron Synchrotron DESY-Zeuthen
Platanenallee 6, 15738 Zeuthen, Germany

**Abstract**

This article addresses the design and construction of modules for the LHCb electromagnetic calorimeter. Quality control and preinstallation tests, including cells pre-calibration, are described and the results of light yield measurements are given.

# 1 Design and construction of ECAL

## 1.1 Introduction

The electromagnetic calorimeter ECAL is part of the calorimeter system [1] of the LHCb detector [2, 3] - a forward single-arm spectrometer (see Fig. 1) for $b$-physics precision studies at LHC.

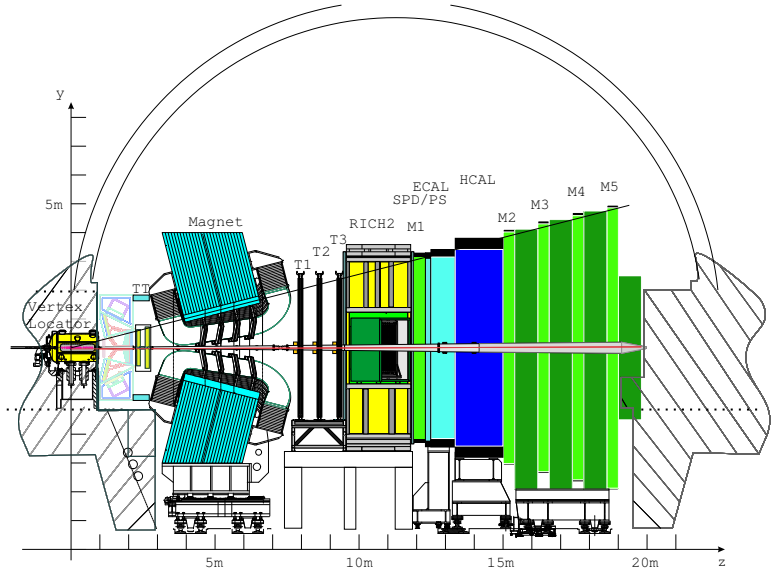


Figure 1: The LHCb detector

The main goals of the ECAL in the LHCb experiment are:

- to provide energetic cluster candidates for the zero level L0 trigger [4] that selects $b$-containing events;
- to reconstruct photons with a precision sufficient for the reconstruction with good mass resolution of $B$-meson decays including photons or $\pi^0$;

- to participate in particle identification, particularly of electrons, providing a charged hadron rejection of better than 100;

ECAL complies with the following requirements:

- an energy resolution of

$$\sigma_E/E = 10\%/\sqrt{E} \oplus 1\%$$

($E$ in $GeV$) which results in a $B$ mass resolution of 65 $MeV/c^2$ for the $B^0 \to K^*\gamma$ penguin decay with a high-$E_T$ photon and of 75 $MeV/c^2$ for $B^0 \to \rho\pi$ decay where the $\pi^0$ reconstruction is essential;

- a fast response within 25 $ns$;

- a good reliability to operate for decades in a radiation hostile environment ( 0.25 $Mrad/year$ in the innermost region) [5].

## 1.2 ECAL design

The LHCb ECAL employs the Shashlik calorimeter technology [6] consisting of a sampling scintillator/lead structure read out by plastic wavelength shifting (WLS) [2, 3] fibers. This technique is well suited to achieve the performance requirements stated above. The experience accumulated by other experiments [7, 8, 9] demonstrates the reliability of the solution at relatively moderate overall cost.

The principal parameters of the ECAL are listed in Table 1.

The ECAL is subdivided into three sections - inner, middle and outer - made of modules of different granularity in order to account for the steep radial dependence of hit density that varies by two orders of magnitude over the active calorimeter surface. The acceptance of the ECAL matches projectively that of the tracking system, $\theta_x < 300\ mrad$ and $\theta_y < 250\ mrad$, and is limited to $\theta_{x,y} > 25\ mrad$ around the beam pipe due to the substantial radiation dose level. The detector is built in two separate halves from individual modules that are positioned in layers on two movable platforms and fixed to a surrounding frame.

Table 1: *Principal parameters of the LHCb electromagnetic calorimeter*

| | |
|---|---|
| Technology | Shashlik |
| Scintillator | $PSM-115\ \oplus\ 2.5\%\ p-terphenyl\ \oplus\ 0.01\%\ POPOP$ |
| Absorber | Lead |
| Volume ratio $Pb:Sc$ | $2:4$ |
| Moliere radius | $3.5\ cm$ |
| Radiation length | $1.64\ cm$ |
| Depth | $42\ cm\ (\ 25\ X_0\ )$ |

The main characteristics of the ECAL structure are given in Table 2. Note that some of the cells closest to the beam are subjected to severe radiation damage and therefore not equipped with photomultipliers.

Table 2: *Main characteristics of the LHCb electromagnetic calorimeter structure*

| | Inner section | Middle section | Outer section |
|---|---|---|---|
| Inner size, $x \times y,\ cm^2$ | $65 \times 65$ | $194 \times 145$ | $388 \times 242$ |
| Outer size, $x \times y,\ cm^2$ | $194 \times 145$ | $388 \times 242$ | $776 \times 630$ |
| Cell size, $cm^2$ | $4.04 \times 4.04$ | $6.06 \times 6.06$ | $12.12 \times 12.12$ |
| # of modules | 176 | 448 | 2688 |
| # of channels | 1472 | 1792 | 2688 |
| # of cells per module | 9 | 4 | 1 |
| Fiber density, $cm^{-2}$ | 0.98 | 0.98 | 0.44 |

## 1.3 Module design

The ECAL module (Fig. 2, 3) consists of a Lead/Scintillator stack structure, fibers, a fiber protection cover on its front side, a fiber bundle and its fiber protection cover on its rear side. The light is read-out from the bundle by a photomultiplier (PMT) at the rear side of the module. The response of the PMT's and electronics is monitored

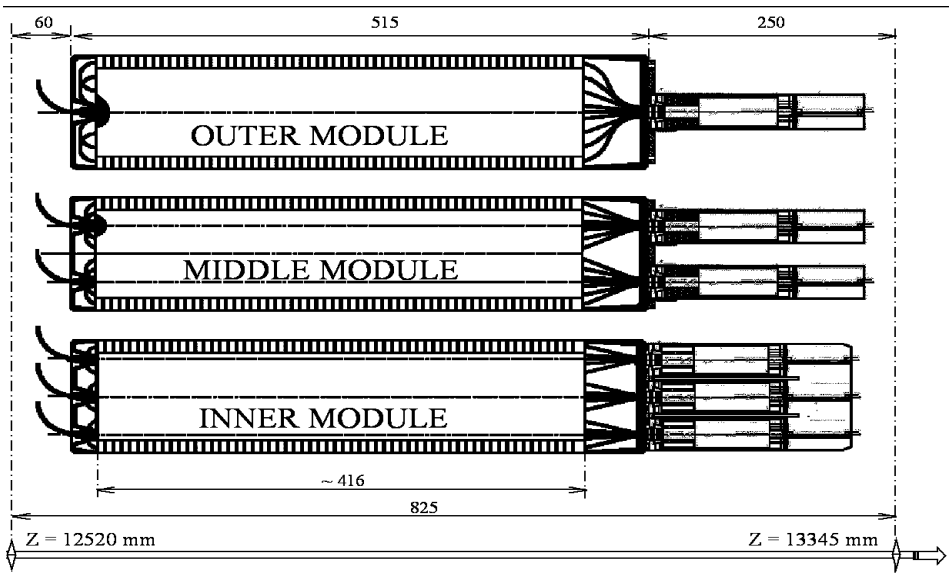


Figure 2: Design of the outer, middle and inner type modules.

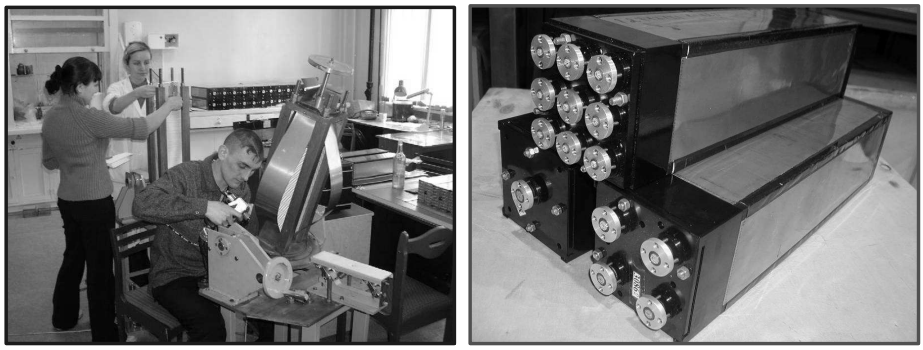

Figure 3: *Left:* Assembly of the module stack at the Vladimir site; *Right:* Outer, middle and inner type modules.

with light from a system of LED's, each LED illuminating several modules. The light from the LED is conveyed to an optical connector on the front face of each module by long clear fibers. From there, a second clear fiber that traverses the module and is merged into the WLS bundle at the back of the module brings the light to the PMT.

A module stack is built from alternating layers of 2 $mm$ thick lead and 4 $mm$ thick scintillator tiles interleaved with white reflecting 120 $\mu m$ thick TYVEK paper (Fig. 4, $left$). On the stack edges black paper angle elements are placed to ensure light tightness. The stack is held together on the four sides by 100 $\mu m$ stainless steel

bands.

The scintillator tiles are produced from polystyrene [1] doped with 2.5% p-terphenyl [2] and 0.01% POPOP [3]. The light from the scintillator tiles is absorbed, re-emitted and transported by 1.2 *mm* diameter WLS fibers traversing the entire module. The fibers are bundled behind the stack for each individual detector cell. In order to improve light collection efficiency and lateral uniformity of response, the fibers form U-shape loops (Fig. 2, 4, *right*) at the front side of the module, thus each fiber traverses

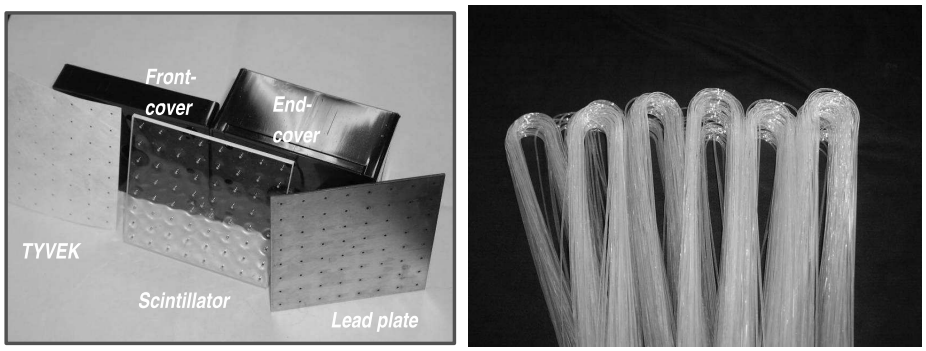


Figure 4: *Left:* Scintillator tile, lead plate and TYVEK paper components of the stack. Also shown are the housings for fiber loops on the front of the module and for fiber bundles at the rear side of the module; *Right:* Fiber loops ready for their insertion in the ECAL modules.

the module twice. The larger density of fibers in the inner and middle sections (see Table 1) is required to provide a sufficient amount of light, while the lower density in the outer section is a compromise between a reasonably sized fiber bundle and a more uniform transverse response [10]. Radiation tolerant multicladding 1.2 *mm* fibers KURARAY Y11(250) [11] are used in the light collection system. They have an absorbtion spectrum peak around wavelengths of 420 *nm* and an emission peak of about 495 *nm*. The core material is polystyrene. At the back of the module

[1]Polystherene in pellets, Polystyrol 165H, [Cn Hn], product of BASF AG, Badische Anilin- & Soda Fabrik Aktiengesellschaft, Carl-Bosch-Atrasse 38, D-67056 Ludwigshafen, Germany.

[2]PTP, p-Terphenyl, 1,4-Diphenylbenzene, [C6 H5 C6 H4 C6 H5], product of FLUKA(TM), Sigma-Aldrich Chemie GmbH, CH-9470, Buchs, Switzerland.

[3]POPOP, 1,4-Bis(5-phenyl-2-oxazolyl)benzene, [C24 H16 N2 O2], product of FLUKA(TM), Sigma-Aldrich Chemie GmbH, CH-9470, Buchs, Switzerland.

the fibers are also bent to form a bundle. The 1.2 $mm$ diameter KURARAY Clear-PSMS-40 clear fiber brings the LED light from the optical connector at the front side of the module to the bundle behind each cell. The bundles have an effective diameter varying from 6.0 $mm$ for the inner modules to 10.8 $mm$ for the outer ones. To reduce the contribution from the PMT photocathode non-uniformity to the energy resolution constant term, a rectangular polystyrene light mixer is placed between the fiber bundle and the PMT window. The dimensions of the light mixer were chosen from MC simulations. Given a photocathode non-uniformity of 20 % a light mixer with $l = 32\ mm$ and $h = 8\ mm$ results in a response non-uniformity of 0.1 % which is small compared to a 1 % constant term of the energy resolution [12].

The light is read out by Hamamatsu R7899-20 photomultipliers [13] each one inside a permalloy protection tube, and connected to a Cockcroft-Walton (CW) voltage multiplier (Fig. 5).

Figure 5: Hamamatsu R7899-20 photomultiplier together with the light mixer, mixer housing and permalloy magnetic screen (left) and the Cockcroft-Walton multiplier connected to a PMT (right)

The overall length of the assembled stack including the related mechanics is 416 $mm$. The whole ECAL system including the stack, fiber loops protection, connection of clear monitoring fibers at the front side and light readout and cabling at the rear side occupies in total 825 $mm$ along the beam direction.

## 1.4 Manufacture of the ECAL modules

Module assembly is illustrated in Fig. 6 for the inner modules.

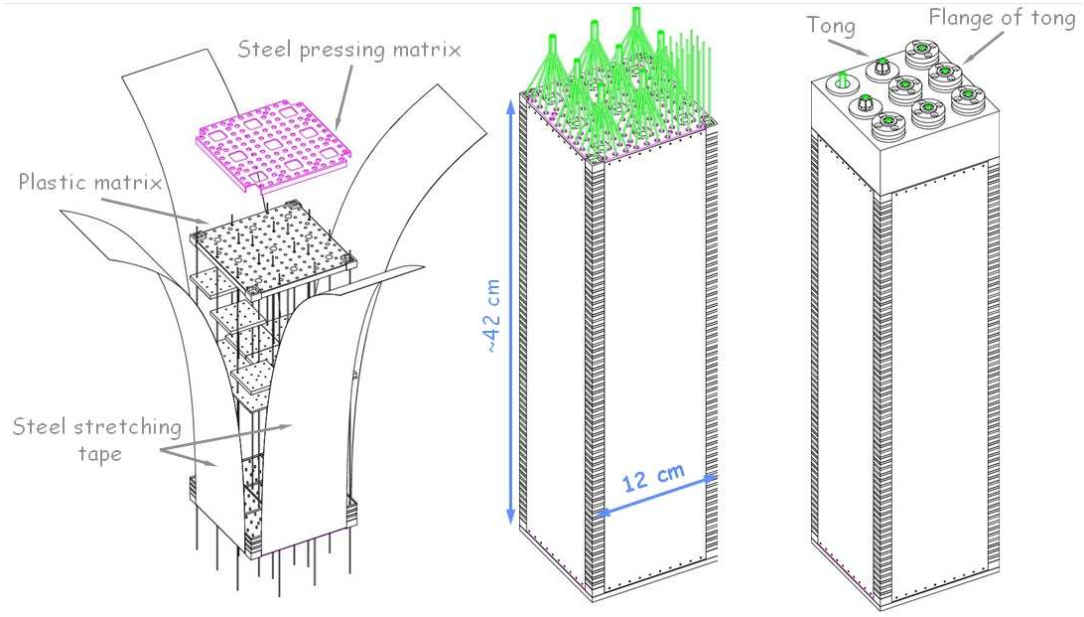


Figure 6: Assembly of the inner type module

The lead plates for the modules are produced using sheet-metal stamping. An additional coating layer of tin a few $\mu m$ thick ensures the rigidity of the plates. The high precision of fiber holes positioning is important to prevent the fiber cladding from being scratched upon insertion.

Scintillating tiles are produced using the high pressure injection molding technique. Tile edges are chemically treated thus providing diffusive reflection in order to improve light collection efficiency, lateral uniformity and prevent tile-to-tile light cross-talk. This technique of tile edges treatment ensures better light collection efficiency and lateral uniformity of response compared to the $Al$ evaporation in vacuum by HV-induced explosion [7, 10].

The Pb/Sc tiles are first stacked in the vertical position using tooling that ensures correct alignment of the fiber holes. The first and the last tiles are steel pressing matrix plates. The stack is then compressed with a 500 $kG$ force. The compression is repeated until no further deformation is observed. To ensure overall construction rigidity stainless steel bands of 100 $\mu m$ thickness are welded to the steel matrix

plates on four sides.

Prior to be inserted in the stack, the WLS fibers are cut, and the U-shape loops are produced. The fiber loops have a radius as small as 10 $mm$ in the inner section modules. This is far below the minimum recommended by Kuraray. The dedicated bending procedure lasts about 15 minutes in a dry uniform heat at a temperature of about 80°C. After insertion into the stack structure the fibers are also bent to form a bundle at the rear side of the module. In this case the radii are always greater or equal to 30 $mm$ therefore no special efforts are needed. The fiber bundle is protected by a fiber housing and fixed with tongs. Finally the fiber bundle is fly-cut to ensure a flat surface of the fiber ends and a good optical contact with the PMT.

## 1.5 Calorimeter wall design

At the assembly stage, calorimeter modules are piled up on two movable platforms, one on each side of the beam line (Fig. 7).

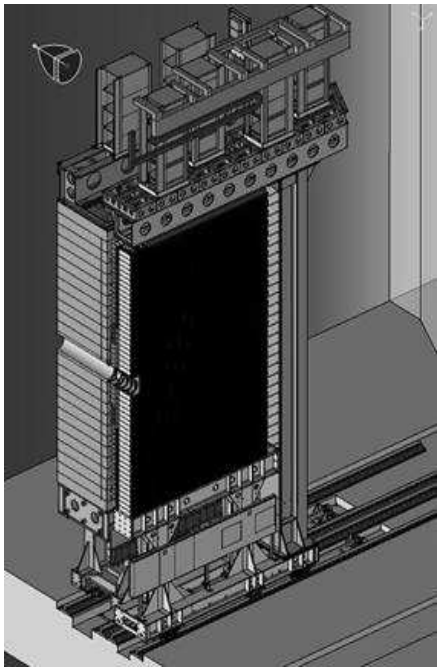

Figure 7: Structure of one half of the ECAL detector

On each of the platforms modules are grouped in two-row structures each compressed with a stainless steel band of 0.1 $mm$ thickness and 400 $mm$ width. Strips

of steel tape of the same size are placed in between the two rows inside a double row structure to ensure a uniform load distribution. Each group is compressed with a dedicated mechanical tool with respect to the side metallic frame to ensure a dense (adjusted) packing and positioned along the $x$-coordinate as a unit structure in order to precisely align the edge at $x = 0$, the nominal beam position.

The 48 innermost modules subjected to the highest radiation dose, could need to be substituted if the radiation induced degradation significantly affects their performance. To allow this replacement the design of the four central vertical columns is different. The modules belonging to this area as well as the modules on top of them are grouped in two double columns, and each is stretched vertically similarly to the treatment of horizontal double rows.

The platform housing the front end electronics and part of the system firing LEDs to monitor the read-out chain stability and to control LED stability with precise pin-diodes, is located on top of the detector. The main part of the monitoring system as well as the system to set, distribute and control the voltage, is positioned inside the platform supporting the calorimeter.

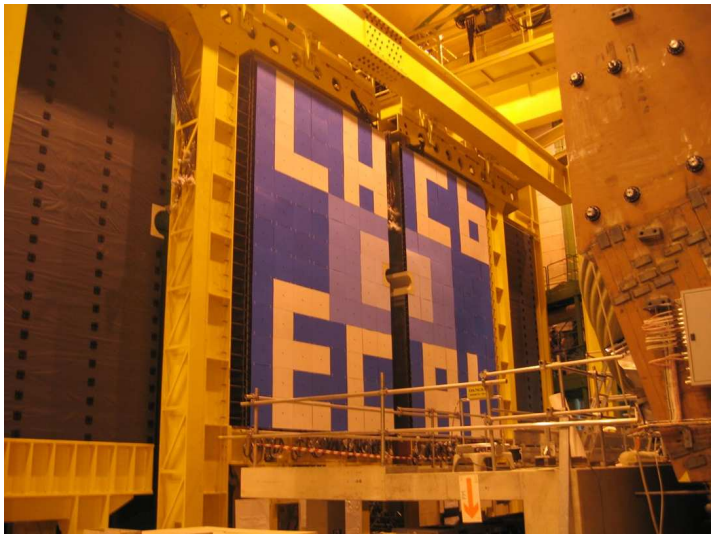

Figure 8: Assembled ECAL detector

The calorimeter module wall has been assembled and instrumented at CERN (Fig. 8). The size of the wall structure is within 1 $mm$ equal to the design value.

# 2 Quality control of module components

## 2.1 Overview

Quality control at the stage of module production includes the following steps:

- control of material arriving from the manufacturer to ensure its compliance with specifications, incoming material control;
- tile light yield tests;
- quality control after the chemical treatment of tile edges;
- fiber quality control measurements;
- overall module performance tests.

All control measurements are based on the comparison of the result of individual measurements with nominal values obtained from a reference item which performance is carefully studied by measurements with more precise techniques (spectroscopy, test beams, etc.).

## 2.2 Incoming raw material control

- Polystyrene control

    1. Admixtures level. This test is based on the infrared spectroscopy technique, which is developed to analyze the composition of organic substances. Since different chemical bonds correspond to different resonance frequencies any deviation from the reference pattern signifies the presence of admixtures which can lead to undesirable shifts in materials' absorbtion and fluorescence spectra (see Fig. 9). Even tiny irregularities such as different geometric isomerism can lead to significant effects. The size of the effect allows also the quantitative estimates of the admixtures level. The specimen is taken out mechanically and dissolved in chloroform. This method gives an accuracy of about 1%.

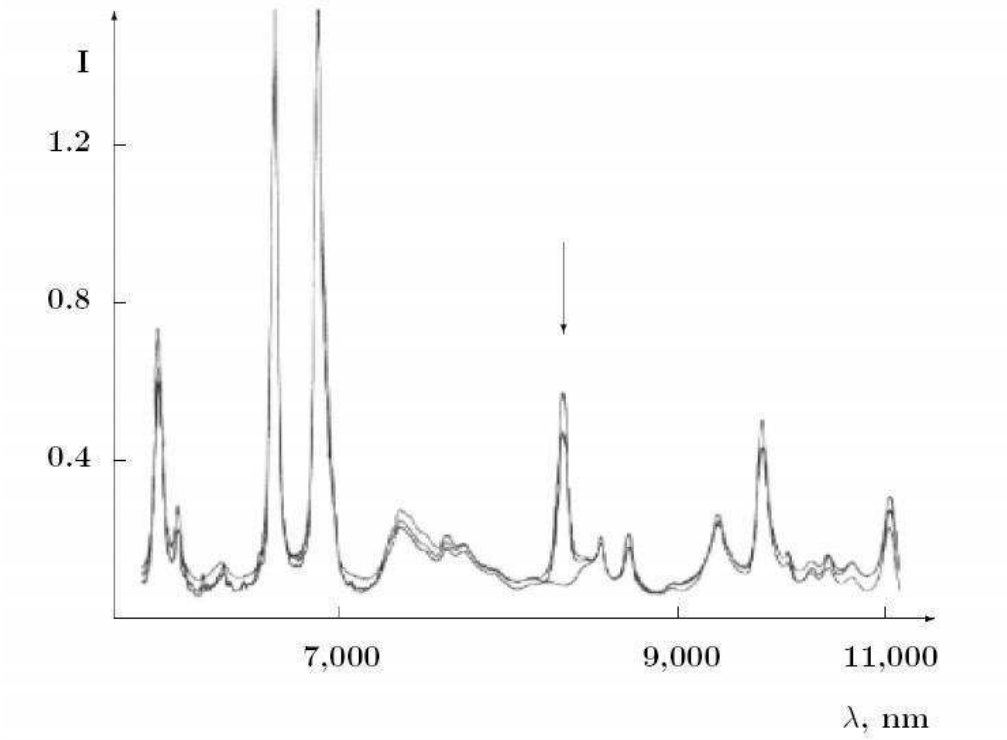


Figure 9: The infrared spectra for three samples of plastic. The pure polystyrene sample has no peak in the region indicated by an arrow.

2. "Transparency" control. In this test the dependence of the response of polystyrene on the wavelength of incoming light is measured with a spectrophotometer. Each tile is measured at 10 points uniformly distributed over its surface. Special attention was paid to the transparency for light with $\lambda = 420nm$, since the scintillator emits the light of this wavelength. To account for losses due to the partial reflection the reference value measured at $\lambda = 590nm$ (at this value absorption is closed out completely) is subtracted.

- P-terphenyl and POPOP. They are also subjected to a double ray spectrometer test. The first ray goes through the reference sample, the second one - through the test sample allowing to measure any discrepancy between the absorption spectra of the two samples. If it is greater than 2-3% the sample is rejected.

### 2.2.1 Tile production control

From each molding series 30% of the tiles are measured. If their performance has only a small deviation from a reference tile and the spread over the tiles is less than 5% the whole batch passes quality control.

At first a spectrophotometer control ensures transparency to the blue light. On average 5.8% of light at 420 $nm$ is lost with an RMS of the distribution of 0.5%. The transparency variations within one plate is as small as 5%.

The setup of the next test comprises a scintillator plate to be measured and fibers coming through its holes and forming a bundle in front of a PMT. The plate is illuminated with a constant light source and the response from fibers is measured. Tiles with light yield differing from the standard value by less than 5% are accepted for further processing.

The scintillator tile is subjected to the same test once again after the matting of edges since the quality of edge matting influences significantly the light yield uniformity of the response from a tile.

The results of outer tile measurements are presented in Fig. 10. Unmatted tiles (on the left) have a lower light yield compared to matted ones by a factor of 2. Furthermore the tile-to-tile spread for unmatted tiles is about 1.5% while for the matted it is about 2.5%. The tiles with marginal light yield are installed in the same module to minimize tile-to-tile spread within a module. For inner and middle modules the tile-to-tile spread was found to be 6% and 5% respectively.

## 2.3 WLS fibers control

Wavelength shifting fibers should match the following requirements:

- an attenuation length, $L_{att} > 90$ $cm$ for a length range of 15-70 $cm$. The relative dispersion (RMS/average) of the fiber attenuation length should be less than 10%;

- a light yield relative dispersion of less than 5%;

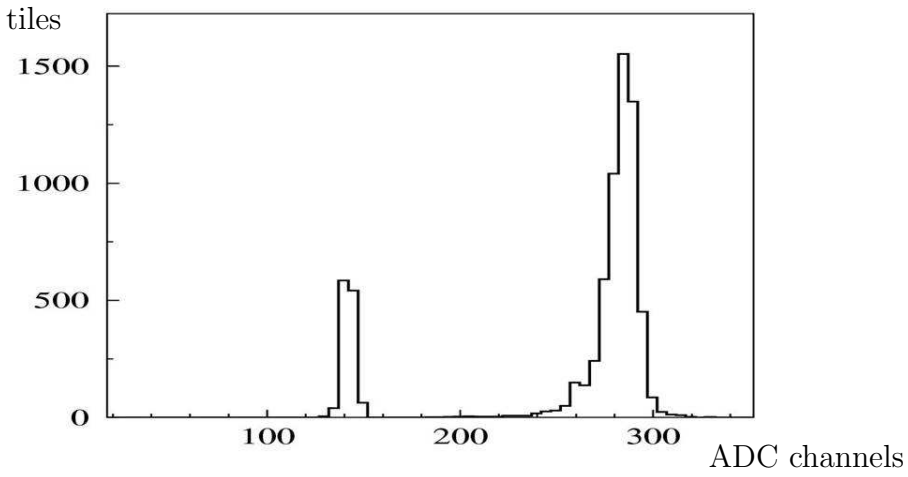


Figure 10: Light yield in scintillating tiles of the outer type. The left and right peaks correspond to the tiles before and after matting respectively. The difference in the number of entries in the two peakss is due to the different quantity of measured tiles.

- a decay time, of less or about 8 $ns$;
- a sufficient radiation resistance [14].

All the essential quality checks were carried out by the manufacturer. Before the fiber loops production fiber-to-fiber variation was studied by illuminating with a radioactive source a tile with the fiber under test inserted in it. It was found that fiber-to-fiber spread is less than 2% including the measurement error, in good agreement with the specifications (see Fig. 11).

The important parameters were studied again after the bending procedure. First the efficiency of light passage through a loop was studied (see Fig. 12). A scintillating tile was threaded on the fiber and placed on one side of the fiber just before the loop. The fiber was illuminated through the tile. To reach the two ends of the fiber the light had to travel through the loop and a straight part of the fiber in one case and just through a similar length straight part in the other case. The ratio of these two light yields was taken as a measure of the light losses in the loop and is presented

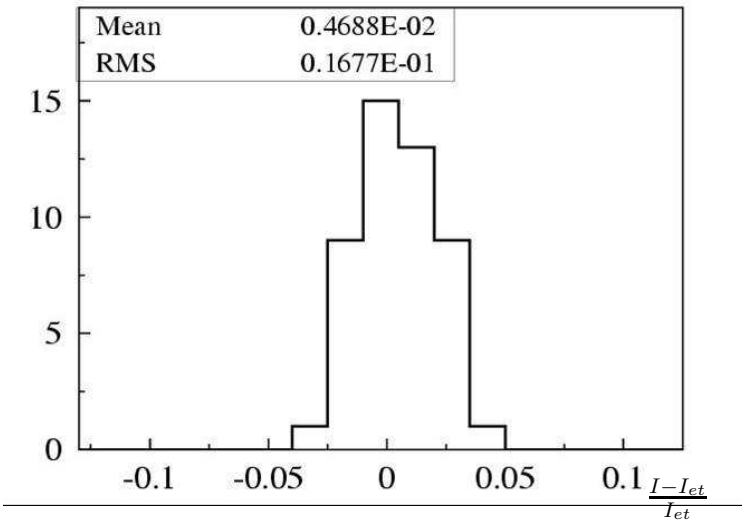


Figure 11: Fiber-to-fiber light yield spread.

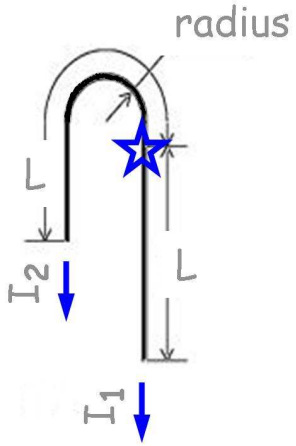


Figure 12: The schematic model of loop measurements.

in Fig. 13 for a group of fibers. It amounted to 5.5% on average. The loop-to-loop spread was measured by comparing the light yield of a tested fiber to that of a standard fiber. It was measured to be 2% and corresponds to the fiber-to-fiber spread with a good precision. This demonstrates that the loop did not introduce any additional spread.

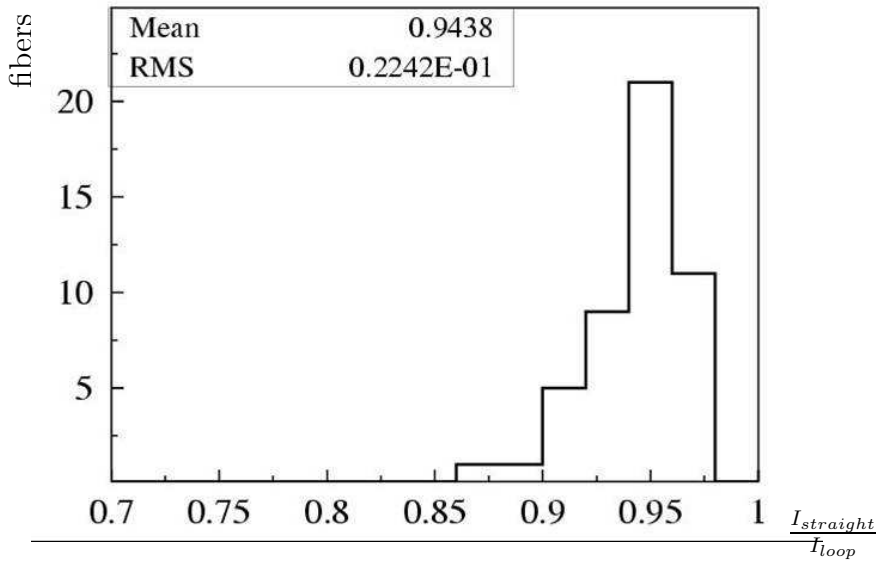


Figure 13: Measure of the decrease in intensity introduced by the loop in the fibers using the technique explained in the text.

# 3 Quality control and precalibration of ECAL modules with cosmic particles

The express test of module quality measurements was held at the production site. The modules placed in a horizontal position were studied using the cosmic rays to measure their response to minimum ionizing particles. This measurement lasted only half an hour for an individual module. Particles were crossing the cell at all angles, with the majority of them depositing a small energy in it, thus yielding a reasonable precision for only modules with the biggest cell size (Fig. 14). The width of the distribution was found to be 5%.

The final quality control of the ECAL cells was made after transportation at CERN using the cosmic rays. The test bench was a lightproof chamber where a batch of modules was placed vertically in between two layers of scintillator counters to provide a trigger for a cosmic ray (see Fig. 15).

The readout of an individual cell was through a PMT with a light mixer in front of the photocathode window. A unique set of photomultipliers together with Cockcroft-Walton bases was used for all measurements. The photomultipliers were

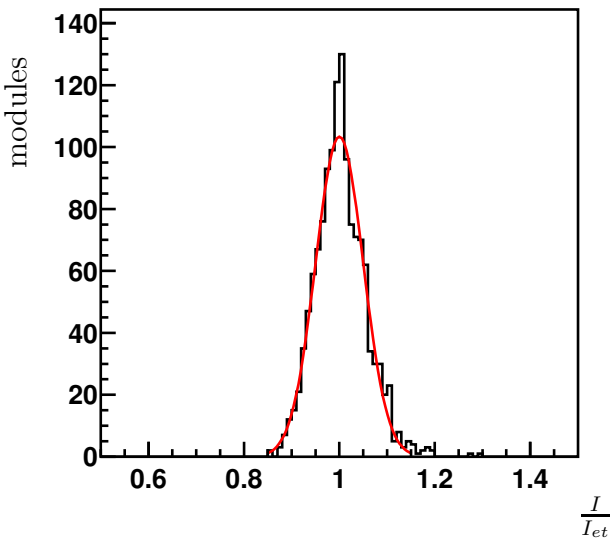


Figure 14: Normalized response of the horizontally positioned outer modules to cosmic rays.

selected to have the same photocathode efficiency within 5%. The time stability was monitored by the LED light. The light from LED was delivered to the PMT by a dedicated U-shape clear fiber protected by a metal housing as shown in Fig. 16. The signal from each cell was digitized by a 12-bit ADC with a sensitivity of 0.25 pC/channel. A dedicated software allowed to set PMT HV, to perform DAQ and to control LEDs.

The PMT gain was set to $10^6$ in order to have enough sensitivity to the minimum ionizing particles. The gain $G$ of each phototube was estimated through the response to the LED signal using the following formula:

$$G = \frac{\sigma_{led}^2 \times s_{adc}}{A_{led} \times q_e \times f}$$

with

- $A_{led}$ and $\sigma_{led}$, respectively, the amplitude and width of the LED signal as read by the ADC,
- $s_{adc}$, the sensitivity of the ADC, 0.25 $pC/channel$,
- $q_e$, the charge of the electron,

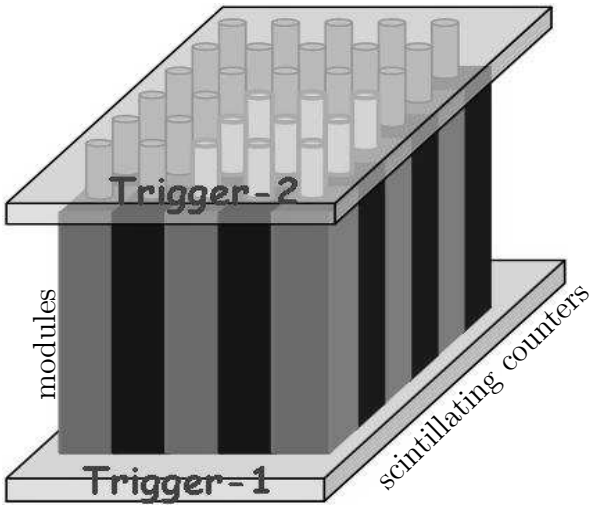


Figure 15: Schematic representation of the cosmic setup.

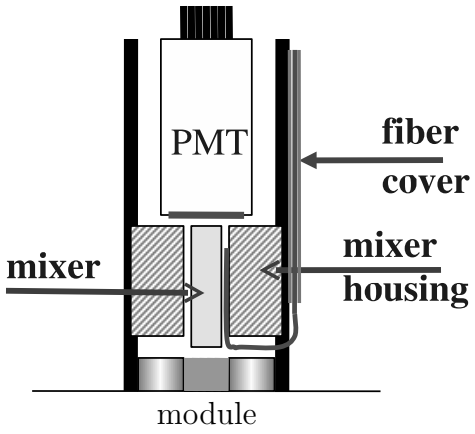


Figure 16: Schematic representation of the module readout.

- $f$, the Fano factor taken to be 1.2.

For each module batch three data samples were collected: a general run with cosmic trigger preceded and followed by short runs with flashing LED to monitor the PMT gain. The cosmic run duration to collect significant peaks for the inner, middle and outer module types was respectively 22 hours, 6 hours and 1 hour per batch due to the difference in the solid angle containing all the particles fully traversing the cell.

During the offline analysis, the selection algorithm required minimal energy de-

position in all cells surrounding the local energy deposition maximum in order to avoid broadening of the MIP distribution due to tracks traversing several cells. This sharpened the distribution of all cells, but the ones that benefited most were cells that were completely surrounded by other cells, a maximum of eight (Fig. 17, $left$). For corner cells only 3 adjacent cells could be vetoed thus introducing a low energy tail in the distribution (Fig. 17, *right*). The resulting distributions were fit

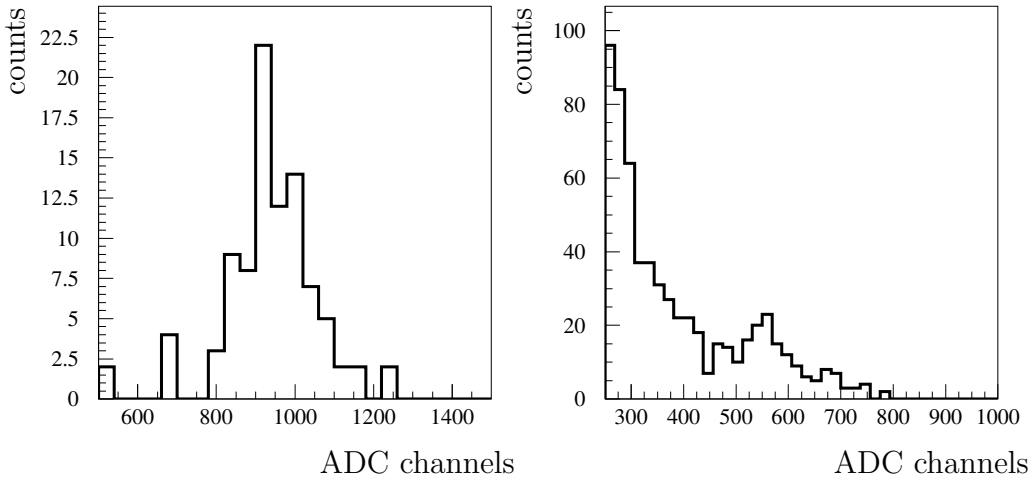


Figure 17: Inner cells precalibration. *Left:* The energy deposition in a central cell for vertical muon tracks; *Right:* the energy deposition in a corner cell.

to a gaussian plus a polynomial background of the second order to obtain the MIP position.

All cells with energy deposition outside three standard deviations were remeasured in additional runs. If the result was reproduced the module was rejected (see Table 3).

Table 3: *Results of the quality control.*

| Module type | Number of cells | Outside 3 $\sigma$ |
|---|---|---|
| **INNER** | 1935 | 12 |
| **MIDDLE** | 1798 | 2 |
| **OUTER** | 2790 | 4 |

The photocathode efficiency of the photomultiplier, the ADC gain but mostly the geometry of the phototube and mixer introduce a spread in the overall response of the read-out channels. The required correction coefficients were determined by averaging over a large number of cells measured with the same readout channel. Time drift of the response of individual read out channels over all the measurements of a given module type was also studied (see Fig. 18), approximated with a linear function and corrected for each data sample. The distribution of all MIP values,

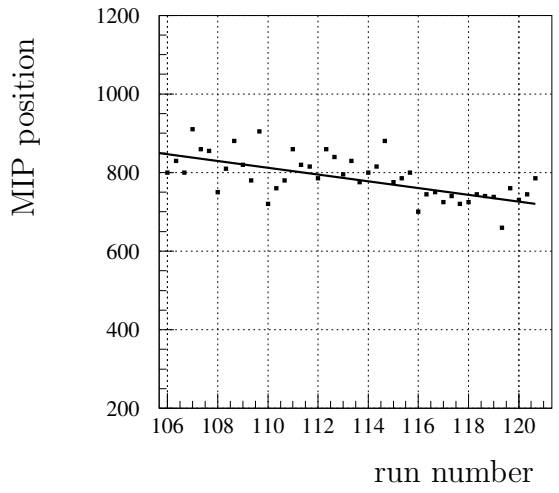


Figure 18: The time dependence of the MIP position for a typical electronic channel over all the middle module runs.

after applying these corrections, is shown in Fig. 19 for the three cell types.

Whenever any cell had to be remeasured, the whole module was tested again. This provided a second set of data for 368 inner and 24 middle cells that allowed to estimate the measurement error. In both cases the precision of the measurement is seen to be within 3%. It was therefore assumed to have the same value for the outer modules. The spread of mip distributions for the three types of modules is given in Table 4 before and after unfolding this measurement error.

The response of the LHCb ECAL modules to a MIP has also been measured in a test beam to be equivalent to that of a 0.33 $GeV$ electron. Based on this number the

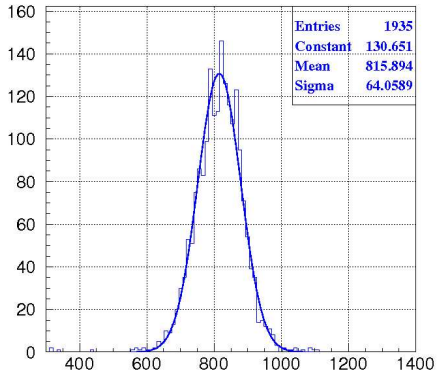


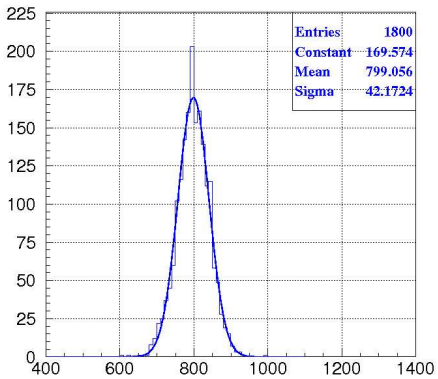


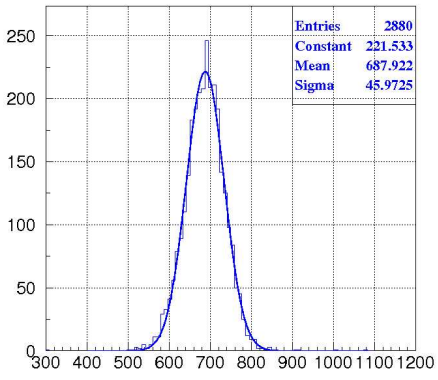


Figure 19: The distribution of the mean energy deposition of minimum ionizing particles in the cells of different module types.

Table 4: *The standard deviations of the mean energy deposition by minimum ionizing particles in the three cell types, before and after taking into account the measurement error.*

| Module type | Precalibration coefficients spread | Cell-to-cell spread |
|---|---|---|
| **INNER** | 8.0% | 7.4% |
| **MIDDLE** | 5.3% | 4.4% |
| **OUTER** | 6.7% | 6.0% |

light yield, the number of photoelectrons per GeV of deposited energy, $N_{ph.e.}/GeV$, was calculated for the cells of the three module types. For each cell the number of photoelectrons recorded for the LED signal was estimated using:

$$N_{ph.e.}(LED) = \left(\frac{A(LED)}{\sigma(LED)}\right)^2 ,$$

where $A(LED)$ and $\sigma(LED)$ are expressed in the ADC channels. Then

$$N_{ph.e.}/GeV = N_{ph.e.}(MIP) \,/\, 0.33\,GeV = \frac{A(MIP)\cdot A(LED)}{\sigma^2(LED)\cdot 0.33\,GeV} ,$$

where $A(MIP)$ is the amplitude of the response to MIP in the ADC channels. This gives for inner cells about 3100 $ph.e./GeV$ of deposited energy, 3500 - for middle and 2600 for outer. The difference is due to different WLS fibers density in inner/middle and outer modules and the difference in cell size that affects the probability of photon absorbtion in the scintillating tiles. These values are in a good agreement with the test beam light yield measurements.

# 4 Conclusion

The modules for the Shashlik type electromagnetic calorimeter for the LHCb experiment have been designed, manufactured and installed. Several quality tests have been carried out at the various stages of manufacturing and construction to ensure its designed performance. A preinstallation test with cosmic rays has demonstrated that the spread in the ECAL cells response is within 8%.

# References


[1] LHCb Calorimeters, *Technical Design Report*, CERN/LHCC/2000-0036.

[2] LHCb Technical Proposal, CERN LHCC 98-4 LHCC/P4, (1998).

[3] LHCb Reoptimized Detector, Design and Performance, *Technical Design Report*, CERN/LHCC/2003-030.

[4] LHCb Trigger System, *Technical Design Report*, CERN/LHCC/2003-031.

[5] Radiation damage of LHCb electromagnetic calorimeter, LHCb 2000-033.

[6] G.S.Atoyan *et al*, *Nucl.Instrum.Meth.* **A320** 144 (1992);
J.Badier *et al*, CMS TN/92-45 (1992).

[7] HERA-B Proposal, DESY-PRC 94/02, (1994);
HERA-B Design Report, DESY-PRC 95/01, (1995).

[8] A.Bazilevsky *et al*, *IEEE Transactions on Nuclear Science* v.43, No.3 (1996).

[9] J.Badier *et al*, *Nucl.Instrum.Meth.* **A348** 74 (1994).

[10] Fiber density and uniformity of response of LHCb electromagnetic calorimeter, LHCb 2000-034.

[11] KURARAY Corp., 3-10, Nihonbashi, 2 chome, Chuo-ku, Tokyo, Japan.

[12] Design and construction of electromagnetic calorimeter for LHCb experiment, LHCb 2000-043.

[13] HAMAMATSU PHOTONICS KK, 325-6 Sunayama-cho, Hamamatsu, Shizuoka.

[14] E.Tarkovsky, *Nucl. Instrum. Meth.* **A379**, 515 (1996)